



Aggregation morphology of planar engineered nanomaterials

S. Drew Story^a, Stephen Boggs^a, Linda M. Guiney^b, Mani Ramesh^b, Mark C. Hersam^b,
C. Jeffrey Brinker^c, Sharon L. Walker^{a,d,*}

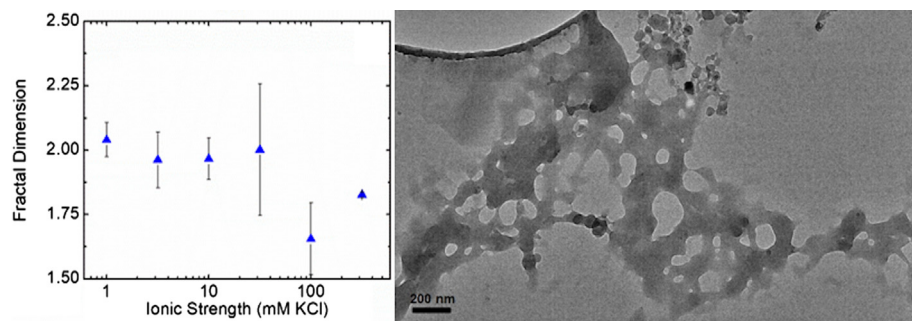
^a Department of Chemical and Environmental Engineering, University of California, Riverside, CA, USA

^b Departments of Materials Science and Engineering, Chemistry, and Medicine, Northwestern University, Evanston, IL, USA

^c Department of Chemical and Biological Engineering, University of New Mexico, Albuquerque, NM, USA

^d Department of Civil, Architectural, and Environmental Engineering, Drexel University, Philadelphia, PA, USA

GRAPHICAL ABSTRACT



Graphene Oxide Engineered Nanomaterial Fractal Dimensions Measured via SLS and Cryo-TEM

ARTICLE INFO

Article history:

Received 1 August 2019

Revised 15 November 2019

Accepted 16 November 2019

Available online 20 November 2019

Keywords:

Aggregate morphology

Static light scattering

Critical coagulation concentration

Fractal dimension

ABSTRACT

In this investigation, the utility of a static light scattering (SLS) technique to characterize aggregate morphology of two-dimensional engineered nanomaterials (2D ENMs) was systematically evaluated. The aggregation of graphene oxide (GO) and lithiated-molybdenum disulfide (Li-MoS₂) were measured and compared to that of a spherical reference colloid, carboxylate-modified latex (CML) nanoparticles. The critical coagulation concentration (CCC) for all dispersions was determined via analysis of aggregation kinetics using time-resolved dynamic light scattering. This technique allowed for the elucidation of the transition from the reaction-limited aggregation (RLA) regime to diffusion-limited aggregation (DLA). The findings of this study support the aggregation trends predicted by Derjaguin-Landau-Verwey-Overbeek (DLVO) theory and recent computer simulations of aggregation kinetics. For all nanomaterials, as ionic strength increased towards the respective CCC, fractal dimension decreased; any increase in ionic strength beyond the CCC did not yield significant change in fractal dimension. Across comparable primary particle sizes and using both carbonaceous (GO) and inorganic (Li-MoS₂) 2D ENMs, this study further supports the use of SLS for the measurement of fractal dimension for 2D materials. To further support this claim, the aggregate morphology of GO in both RLA and DLA regimes was measured via cryogenic transmission electron microscopy.

© 2019 Elsevier Inc. All rights reserved.

* Corresponding author at: Department of Civil, Architectural and Environmental Engineering, Drexel University, Philadelphia, PA, USA.

E-mail address: slw385@drexel.edu (S.L. Walker).

1. Introduction

The rapid increase in the use of planar, or 2-Dimensional, engineered nanomaterials (2D ENMs) for a variety of applications has given rise to the question of whether techniques traditionally used for characterizing environmental fate and transport of colloids, such as light scattering methods, can be applied to 2D ENMs [1–4]. While most light scattering methods assume spherical geometry in their design and interpretation of measurements, this study intends to verify that light scattering techniques, specifically static light scattering (SLS), can be effectively used for colloidal characterization of 2D nanomaterials [5]. The current alternative to traditional methods such as SLS and dynamic light scattering (DLS) is the use of direct visualization techniques, such as transmission electron microscopy (TEM) and cryogenic-TEM. The limitations of these visualization techniques are well documented (sample matrix constraints, limited access to equipment, statistical power, and cost), such that the use of more common light scattering methods would facilitate increased productivity in the environmental nanotechnology community [6].

Two prominent 2D ENMs (graphene oxide (GO) and lithiated-molybdenum disulfide (Li-MoS₂)), as well as a commonly studied spherical model ENM, carboxylate-modified latex (CML) were chosen for this investigation to evaluate the feasibility of using SLS to elucidate aggregate morphology of a colloidal suspension. GO production and usage has increased in a wide variety of consumer and industrial products including electronics, sports accessories, and sensors [7,8]. Li-MoS₂ has likewise grown in popularity for its beneficial characteristics for the development of lithium ion batteries, which include having a high reversible capacity and excellent rate capability [3,9]. While the material, as well as environmental fate and transport characteristics of these materials have been previously assessed, this study is the first of our knowledge to systematically compare the results of two traditional colloidal characterization methods and one imaging technique for 2D ENMs [10–12]. The results of this work provide additional insight into the use of a common light scattering method for studying the environmental behavior of increasingly common planar materials.

2. Materials and methods

2.1. Engineered nanomaterials

The carboxylate-modified latex (CML) nanoparticles used in this study (4% w/v, 0.4 μm) were purchased from Life Technologies (Grand Island, NY). Particle suspensions were made by diluting a stock solution of 4.1 g/mL with deionized water to a concentration of 10 mg/L. This sample concentration was used for all CML particle characterization assays.

The lithiated molybdenum disulfide (Li-MoS₂) and graphene oxide (GO) synthesis methods have been reported previously [13,14]. Briefly, lithiated MoS₂ was prepared by combining 300 mg of bulk MoS₂ powder (American Elements) and 3 mL of butyllithium in a vial, followed by vigorous stirring for 48 h in an argon environment. The slurry was filtered and rinsed extensively with hexane. The MoS₂ was then dispersed in 500 mL of deionized water, followed by bath sonication for 30 min. The unexfoliated material was separated via centrifugation. The top 80% of the supernatant was decanted and dialyzed against deionized water for 7 days to eliminate any residual lithium or hexane. GO was prepared using a modified Hummers' method starting from graphite flakes (3061 grade material from Asbury Graphite Mills, Asbury, NJ). Following oxidation, the GO was rinsed extensively and concentrated via filtration and centrifugation. The GO was then dispersed in deionized water by horn sonication using a Fisher

Scientific Model 500 Sonic Dismembrator (Pittsburgh, PA) with a 1.27 cm tip for one hour at 55 W. Any unexfoliated material was removed by a centrifugation step. The top 80% of the supernatant was decanted and reserved for these studies.

2.2. General characterization of nanomaterials

2.2.1. Electrokinetic properties and aggregation rate of nanomaterials

A ZetaPALS analyzer (Brookhaven Instruments, Holtsville, NY) was used to measure the electrophoretic mobility (EPM) of the nanomaterials. EPM was converted to zeta potential using the Smoluchowski equation [15]. The effective diameter was measured with dynamic light scattering (Brookhaven NanoBrook OMNI, Holtsville, NY) in which measurements were taken at a scattering angle of 90° and a wavelength of 661 nm. It is well understood that even for 3D ENMs there is often a discrepancy in the size values obtained via light scattering versus electron microscopy [1]. For the purposes of this investigation, the ability of the light scattering technique is sufficient to resolve trends in size changes [1]. The influence of ionic strength (IS) on the CML, GO, and Li-MoS₂ nanomaterials was determined by measuring the EPM and effective hydrodynamic diameter across an environmentally relevant IS range of 1.0–100 mM KCl. All electrokinetic and size measurements were taken at room temperature (23 ± 1 °C) and conducted in triplicate.

2.2.2. Aggregate morphology of nanomaterials

The fractal dimensions of the CML, GO, and Li-MoS₂ nanomaterials as a function of IS (1.0–100 mM KCl) were measured using a multi-angle static light scattering instrument (BI-200SM, Brookhaven Instruments, Holtsville, NY) at a wavelength of 633 nm across a scattering angle of 12–45° using 10 logarithmically-spaced increments of the scattering vector. Triplicate measurements were taken using borosilicate glass cuvettes. The fractal dimension values were obtained from the scattering intensities using the Rayleigh-Gans-Debye (RGD) theory and previously described methods

$$I(q) \propto q^{-FD} \quad (1)$$

$$q = \frac{4\pi}{\lambda} \sin \frac{\theta}{2} \quad (2)$$

where $I(q)$ is the scattering intensity as a function of the scattering wave vector, q is the scattering wave vector, FD is the fractal dimension, λ is the wavelength of incident light, and θ is the scattering angle [16,17]. The fractal dimensions of the nanomaterial aggregates were obtained from the slope of the best fit linear line, where the inverse of intensity of the light scattered ($\log(I)$) was plotted against the scattering vector ($\log(q)$). Eq. (1) is a simplification of the more general

$$I(q) \propto F(q)S(q) \quad (3)$$

where $F(q)$ is the form factor and $S(q)$ is the structure factor [18]. The simplified Eq. (1) can be used when the product of q and r_0 is between 10^{-1} and 10^0 , where r_0 is the primary particle radius [19]. The range of angles used to collect intensity values (12–45°) represents a small range of q in order to satisfy this relationship and accommodate the large primary particle radii of the 2D ENMs in this study. A non-integer fractal dimension value from 1 to 3 suggests that the aggregating particles may be fractal, with the lower fractal dimension values correlating with a lower packing density [20]. A lower fractal dimension value typically is a result of fast aggregation occurring amongst similar particles, with the upper spectrum correlating with a maximum density of the aggregate structure as a result from slower aggregation processes [19,21].

2.2.3. Cryogenic transmission electron microscope images of nanomaterials

Cryogenic Transmission Electron Microscopy (cryo-TEM) images were collected of the ENMs on “C-flat” holey carbon films with a mesh size of 200 (Electron Microscopy Services, Hatfield, PA). Before cryo-TEM sample preparation, the EM grids were treated by UV/ozone for two minutes to make the grid surface more hydrophilic. For cryo-TEM sample preparation, Vitrobot (FEI, Hillsboro, OR) was used according to manufacturer’s standard procedures. Briefly, the process parameters in this case were set as: blot time, 4.0 s; wait time, 0 s; and drain time, 0.5 s. To obtain the cryo-TEM images, JEOL 2010 EX HREM (JEOL, Peabody, MA) was operated with a 200 keV accelerating voltage.

3. Results and discussion

3.1. Effects of ionic strength on colloidal stability of engineered nanomaterials

A spherical nanomaterial was chosen to serve as a reference by which to compare and contrast the 2D engineered nanomaterials used in this study. Previous studies have examined the stability of similarly synthesized CML nanoparticles as a function of pH and ionic strength [22]. These stability characteristics, specifically sensitivity of zeta potential and aggregation rate to ionic strength, were verified in this study and used to inform the analysis of the aggregate morphology of the reference CML suspensions.

Consistent with previous findings, Fig. 1 demonstrates that the CML NPs exhibited an increase in zeta potential over a 5-log increase in ionic strength (KCl) at an unadjusted pH of 5.4 ± 0.2 , ranging from -68 mV at 1 mM KCl to -18 mV at 100 mM KCl [22]. Time-resolved dynamic light scattering (TR-DLS) was used to calculate the aggregation rate of the CML NPs. The rate was calculated from the slope of the best fit linear line when plotting effective diameter as a function of time, as done previously by Chen and Elimelech, as well as Stankus et al. and Nason et al. [23–25]. Significant aggregation over a one-hour measurement period occurred at an IS of 64.9 mM KCl and above, reaching a maximum aggregation rate beyond 100 mM KCl (Fig. 2). All aggregation rates were then divided by the maximum rate to determine the overall attachment efficiency, α . These calculated alpha values were then plotted against their respective ionic strengths, yielding a curve that increases steadily before reaching a plateau. The ionic strength at which the increasing portion of the curve intersects the horizontal plateau represents the critical coagulation concentration (CCC) and denotes a transition from the reaction-limited aggregation (RLA) to the diffusion-limited aggregation

(DLA) regime. For the CML NPs, the CCC was found to be 100 mM KCl, as indicated in Fig. 3.

Identical techniques were used to evaluate the stability of the 2D GO and Li-MoS₂ ENMs. While not as sensitive to changes in ionic strength as the CML NPs, the zeta potential of both GO and Li-MoS₂ approached neutrality with greater ionic strength due to a reduction in Debye length. At 1 mM KCl, the zeta potentials of GO and Li-MoS₂ were -20 mV and -25 mV, respectively, increasing to -10 mV and -5 mV at 100 mM KCl (Fig. 1). As a result, the aggregation rates of the planar ENMs increased from zero to a maximum across the range of ionic strengths tested, as determined by TR-DLS (Fig. 2). The CCC values were determined to be 31.6 mM KCl and 50 mM KCl for GO and Li-MoS₂, respectively [26].

3.2. Effects of ionic strength on aggregate morphology of engineered nanomaterials

The aggregation morphology of the colloidal dispersion, as quantitatively described with fractal dimension values acquired from SLS, provides additional insight into colloidal stability beyond zeta potential measurements and overall aggregation rates. Plots displaying fractal dimension as a function of ionic strength, such as those in Fig. 4, are used to qualitatively verify the quantification of the CCC made by analysis of the plots in Fig. 3, thus indicating the RLA-DLA transition. The plots in Fig. 4 are limited to this qualitative interpretation by the large experimental error, which can be attributed to the heterogeneity of the effective hydrodynamic diameter of the ENM dispersions used in this study, coupled with the relatively small range of the scattering wave vector discussed previously. For the CML NP dispersion in the RLA regime, (ionic strength < 100 mM KCl), the fractal dimension values were between 1.375 and 1.5, with an average of 1.45 (Fig. 4). In the DLA regime (ionic strength \geq 100 mM KCl), the fractal dimension values were significantly lower, with an average of 1.26. This result is in-line with previous studies using this technique for similar particle suspensions [26,27].

For GO, in the RLA regime (ionic strength < 31.6 mM KCl), the fractal dimension values measured by SLS were between 1.95 and 2.0, with an average of 1.97 (Fig. 4). In the DLA regime (ionic strength \geq 31.6 mM KCl), the fractal dimension values were lower, with an average of 1.73.

For Li-MoS₂, in the RLA regime, (ionic strength < 50 mM KCl), the fractal dimension value average was 2.2 (Fig. 4). In the DLA regime (ionic strength \geq 50 mM KCl), the fractal dimension values were significantly lower, with an average of 1.73.

To supplement and further verify the fractal dimension measurements from SLS, the fractal dimension of GO in both RLA and DLA regimes was evaluated via analysis of cryo-TEM images

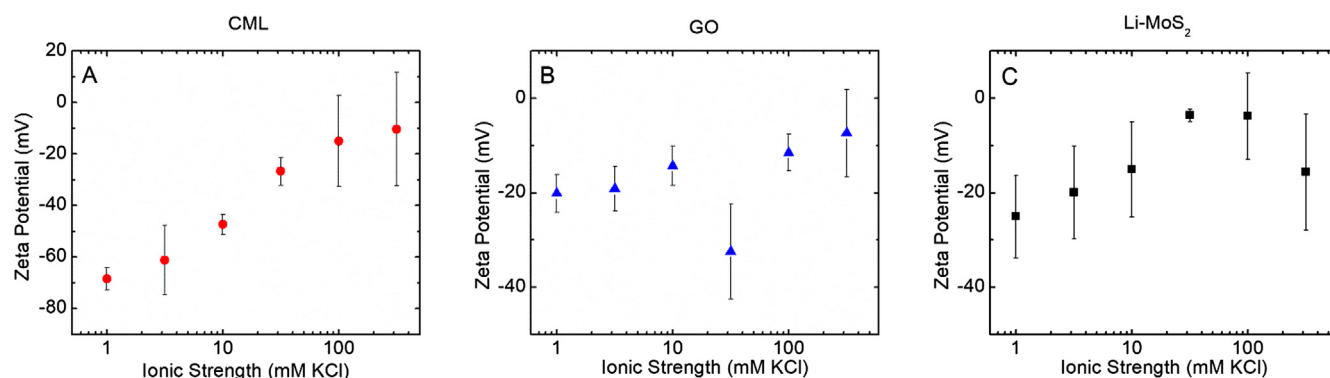


Fig. 1. Zeta potential evaluated as a function of ionic strength for CML (a), GO (b), and Li-MoS₂ (c) ENMs. Concentration of nanomaterials was maintained at 10 mg/L at an unadjusted pH $\sim 5.4 \pm 0.2$. Error bars indicate one standard deviation of triplicate measurements.

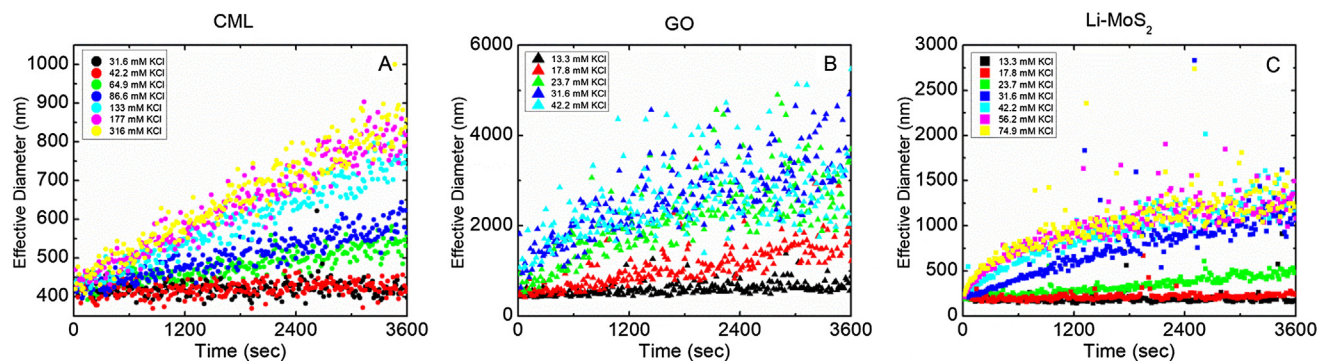


Fig. 2. CML (a), GO (b), and Li-MoS₂ (c) ENMs evaluated as a function of ionic strength and time for effective diameter and aggregation rate. Particle concentration was maintained at 10 mg/L at an unadjusted pH $\sim 5.4 \pm 0.2$.

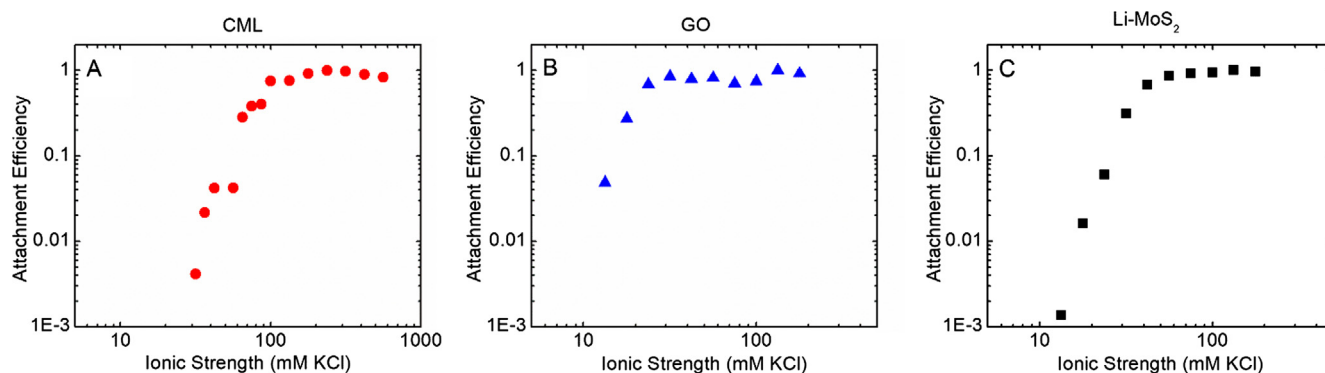


Fig. 3. Attachment efficiency evaluated as a function of ionic strength for CML (a), GO (b), and Li-MoS₂ (c) ENMs.

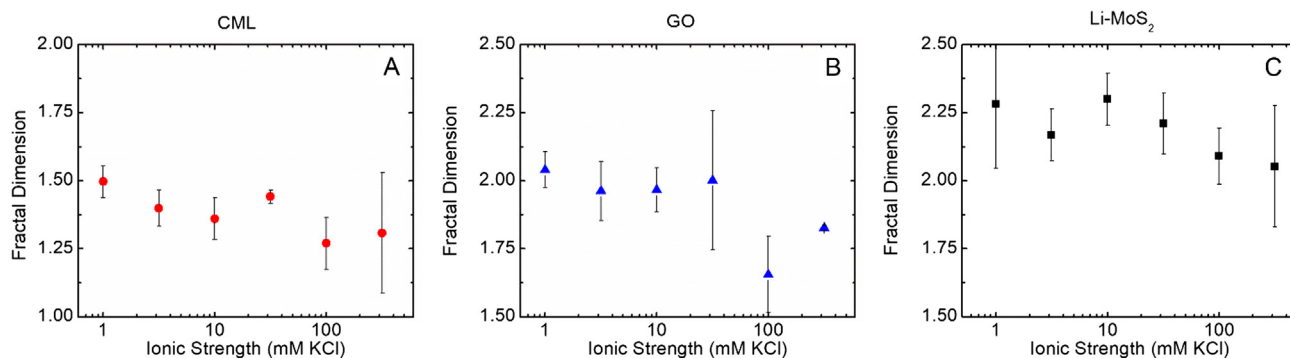


Fig. 4. CML (a), GO (b), and Li-MoS₂ (c) ENMs evaluated as a function of ionic strength for fractal dimension. Particle concentration was maintained at 10 mg/L at an unadjusted pH $\sim 5.4 \pm 0.2$. Error bars indicate one standard deviation of triplicate measurements.

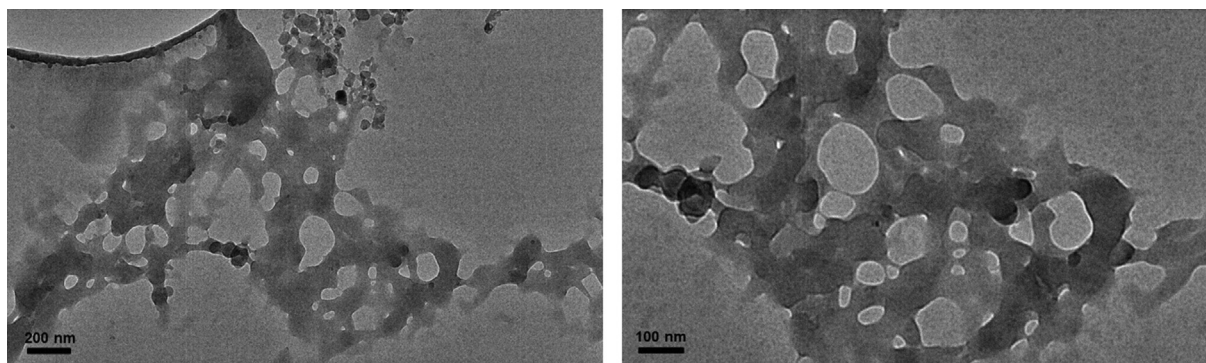


Fig. 5. Micrographs of GO ENMs suspended in 20 mM (left) and 200 mM KCl (right) collected via cryogenic transmission electron microscopy.

(Fig. 5), utilizing ImageJ image processing software. In a 20 mM KCl suspension (below the CCC of 31.6 mM), fractal dimension was 1.96. In a 200 mM KCl suspension (above the CCC), fractal dimension was 1.67. The difference in fractal dimension measured via cryo-TEM between the suspensions corroborates the ability of SLS to distinguish changes in fractal dimension when transitioning from RLA to DLA regimes.

The static light scattering technique qualitatively verified the transition from RLA to DLA, signifying the shift from slow aggregation to fast aggregation, for both spherical and planar ENMs. The fractal dimension values of GO measured using cryo-TEM are in good agreement with those fractal dimension values obtained with SLS. This further supports the deployment of static light scattering for the qualitative characterization of aggregate morphology of planar engineered nanomaterials.

CRedit authorship contribution statement

S. Drew Story: Conceptualization, Data curation, Formal analysis, Investigation, Methodology, Project administration, Visualization, Writing - original draft. **Stephen Boggs:** Data curation, Investigation. **Linda M. Guiney:** Conceptualization, Data curation, Formal analysis, Investigation, Methodology, Writing - original draft, Writing - review & editing. **Mani Ramesh:** Data curation, Investigation, Writing - review & editing. **Mark C. Hersam:** Funding acquisition, Methodology, Project administration, Supervision, Validation, Writing - review & editing. **C. Jeffrey Brinker:** Data curation, Formal analysis, Methodology, Supervision, Writing - review & editing. **Sharon L. Walker:** Conceptualization, Funding acquisition, Investigation, Methodology, Project administration, Supervision, Writing - review & editing.

Declaration of Competing Interest

The authors declare that they have no known competing financial interests or personal relationships that could have appeared to influence the work reported in this paper.

Acknowledgements

This study has been supported by a combination of National Science Foundation (NSF) and Environmental Protection Agency (EPA). S.D. Story was supported by the NSF IGERT: Water SENSE – Water Social, Engineering, and Natural Sciences Engagement Program (Grant # 1144635). S. Walker's participation and the work more broadly were also funded through the UC-CEIN (University of California Center for Environmental Implications of Nanotechnology), which is supported by the NSF and the EPA under Cooperative Agreement Number DBI 0830117. Any opinions, findings, and conclusions or recommendations expressed in this material are those of the author(s) and do not necessarily reflect the views of the NSF or the EPA. This work has not been subjected to EPA review and no official endorsement should be inferred. We would like to acknowledge Dr. Ian Marcus for his efforts editing the manuscript.

References

- [1] C. Levard, E.M. Hotze, G.V. Lowry, G.E. Brown, Environmental transformations of silver nanoparticles: impact on stability and toxicity, *Environ. Sci. Technol.* 46 (13) (2012) 6900–6914.

- [2] O. Lopez-Sanchez, D. Lembke, M. Kayci, A. Radenovic, A. Kis, Ultrasensitive photodetectors based on monolayer MoS₂, *Nat. Nanotechnol.* 8 (7) (2013) 497–501.
- [3] K. Liu, J. Feng, A. Kis, A. Radenovic, Atomically thin molybdenum disulfide nanopores with high sensitivity for DNA translocation, *ACS Nano* 8 (3) (2014) 2504–2511.
- [4] A. Gupta, T. Sakhivel, S. Seal, Recent development in 2D materials beyond graphene, *Prog. Mater. Sci.* 73 (2015) 44–126.
- [5] R.F. Domingos, M.A. Baalousha, Y. Ju-Nam, M.M. Reid, N. Tufenkji, J.R. Lead, G. G. Leppard, K.J. Wilkinson, Characterizing manufactured nanoparticles in the environment: multimethod determination of particle sizes, *Environ. Sci. Technol.* 43 (19) (2009) 7277–7284.
- [6] D. Mähl, J. Diendorf, W. Meyer-Zaika, M. Epple, Possibilities and limitations of different analytical methods for the size determination of a bimodal dispersion of metallic nanoparticles, *Colloids Surf., A.* 377 (1) (2011) 386–392.
- [7] A.K. Geim, K.S. Novoselov, The rise of graphene, *Nat. Mater.* 6 (3) (2007) 183–191.
- [8] G. Brumfiel, Graphene gets ready for the big time, *Nature* 458 (7237) (2009) 390–391.
- [9] T. Stephenson, Z. Li, B. Olsen, D. Mitlin, Lithium ion battery applications of molybdenum disulfide (MoS₂) nanocomposites, *Energy Environ. Sci.* 7 (1) (2014) 209–231.
- [10] J.D. Lanphere, B. Rogers, C. Luth, C.H. Bolster, S.L. Walker, Stability and transport of graphene oxide nanoparticles in groundwater and surface water, *Environ. Eng. Sci.* 31 (7) (2014) 350–359.
- [11] J.D. Lanphere, C.J. Luth, L.M. Guiney, N.D. Mansukhani, M.C. Hersam, S.L. Walker, Fate and transport of molybdenum disulfide nanomaterials in sand columns, *Environ. Eng. Sci.* 32 (2) (2015) 163–173.
- [12] J.D. Lanphere, C.J. Luth, S.L. Walker, Effects of solution chemistry on the transport of graphene oxide in saturated porous media, *Environ. Sci. Technol.* 47 (9) (2013) 4255–4261.
- [13] M.C. Duch, G.R.S. Budinger, Y.T. Liang, S. Soberanes, D. Urich, S.E. Chiarella, L.A. Campochiaro, A. Gonzalez, N.S. Chandel, M.C. Hersam, G.M. Mutlu, Minimizing oxidation and stable nanoscale dispersion improves the biocompatibility of graphene in the lung, *Nano Lett.* 11 (12) (2011) 5201–5207.
- [14] N.D. Mansukhani, L.M. Guiney, P.J. Kim, Y. Zhao, D. Alducin, A. Ponce, E. Larios, M.J. Yacaman, M.C. Hersam, High-concentration aqueous dispersions of nanoscale 2D materials using nonionic, biocompatible block copolymers, *Small* 12 (3) (2016) 294–300.
- [15] M. von Smoluchowski, Versuch einer mathematischen theorie der koagulationskinetik kolloider l. o' sungen, *Z. Phys. Chem.* 92 (1918) 129.
- [16] M.Y. Lin, H.M. Lindsay, D.A. Weitz, R.C. Ball, R. Klein, P. Meakin, Universality in colloid aggregation, *Nature* 339 (1989) 360–362.
- [17] D. Jassby, J. Farner Budarz, M. Wiesner, Impact of aggregate size and structure on the photocatalytic properties of TiO₂ and ZnO nanoparticles, *Environ. Sci. Technol.* 46 (13) (2012) 6934–6941.
- [18] J.S. Pedersen, Analysis of small-angle scattering data from colloids and polymer solutions: modeling and least-squares fitting, *Adv. Colloid Interface Sci.* 70 (1997) 171–210.
- [19] G.C. Bushell, Y.D. Yan, D. Woodfield, J. Raper, R. Amal, On techniques for the measurement of the mass fractal dimension of aggregates, *Adv. Colloid Interface Sci.* 95 (1) (2002) 1–50.
- [20] I. Chowdhury, M.C. Duch, N.D. Mansukhani, M.C. Hersam, D. Bouchard, Colloidal properties and stability of graphene oxide nanomaterials in the aquatic environment, *Environ. Sci. Technol.* 47 (12) (2013) 6288–6296.
- [21] C.J. Brinker, G.W. Scherer, *Sol-Gel Science: The Physics and Chemistry of Sol-Gel Processing*, Academic Press, 2013.
- [22] C. Chen, T. Waller, S.L. Walker, Visualization of transport and fate of nano and micro-scale particles in porous media: modeling coupled effects of ionic strength and size, *Environ. Sci. Nano.* 4 (5) (2017) 1025–1036.
- [23] K.L. Chen, M. Elimelech, Aggregation and deposition kinetics of fullerene (C-60) nanoparticles, *Langmuir* 22 (26) (2006) 10994–11001.
- [24] D.P. Stankus, S.E. Lohse, J.E. Hutchison, J.A. Nason, Interactions between natural organic matter and gold nanoparticles stabilized with different organic capping agents, *Environ. Sci. Technol.* 45 (8) (2011) 3238–3244.
- [25] J.A. Nason, S.A. McDowell, T.W. Callahan, Effects of natural organic matter type and concentration on the aggregation of citrate-stabilized gold nanoparticles, *J. Environ. Monit.* 14 (7) (2012) 1885–1892.
- [26] I. Chowdhury, S.L. Walker, S.E. Mylon, Aggregate morphology of nano-TiO₂: role of primary particle size, solution chemistry, and organic matter, *Environ. Sci. Process. Imp.* 15 (1) (2013) 275–282.
- [27] Z. Meng, S.M. Hashmi, M. Elimelech, Aggregation rate and fractal dimension of fullerene nanoparticles via simultaneous multiangle static and dynamic light scattering measurement, *J. Colloid Interface Sci.* 392 (2013) 27–33.